

## The electronic mechanism of the $\gamma/\gamma'$ interface strength of Ir-based alloys

This article has been downloaded from IOPscience. Please scroll down to see the full text article.

2002 J. Phys.: Condens. Matter 14 10041

(<http://iopscience.iop.org/0953-8984/14/43/303>)

View [the table of contents for this issue](#), or go to the [journal homepage](#) for more

Download details:

IP Address: 171.66.16.96

The article was downloaded on 18/05/2010 at 15:15

Please note that [terms and conditions apply](#).

# The electronic mechanism of the $\gamma/\gamma'$ interface strength of Ir-based alloys

K Chen<sup>1</sup>, L R Zhao<sup>1</sup> and John S Tse<sup>2</sup>

<sup>1</sup> Structures, Materials and Propulsion Laboratory, Institute for Aerospace Research, National Research Council Canada, Ottawa, Canada

<sup>2</sup> Steacie Institute for Molecular Science, National Research Council Canada, Ottawa, Canada

Received 6 June 2002

Published 18 October 2002

Online at [stacks.iop.org/JPhysCM/14/10041](http://stacks.iop.org/JPhysCM/14/10041)

## Abstract

The electronic structures of the  $\gamma/\gamma'$  interface for two-phase Ir-based alloys (Ir/Ir<sub>3</sub>Ta and Ir/Ir<sub>3</sub>Ti) have been investigated by performing first-principles quantum mechanics DMol3 (a type of density functional theory for molecules) calculations. The Mayer bond order (MBO) is used to represent the shear and cohesion strengths of the interface by a local sum of the horizontal and vertical MBOs. By comparison with those for single-crystal Ir, the results show that both the cohesive and shear strengths of the  $\gamma/\gamma'$  interface for the Ir/Ir<sub>3</sub>Ta alloy increase. The cohesive strength of the interface for the Ir/Ir<sub>3</sub>Ti alloy increases, whereas the shear strength of the interface for Ir/Ir<sub>3</sub>Ti decreases. The electron charge density, the Hirshfeld charge, and orbital charge transfers are also calculated and analysed. An electronic mechanism for the  $\gamma/\gamma'$  interface strength of Ir-based alloys is then suggested.

## 1. Introduction

Ni-based single-crystal (SC) superalloys used for turbine blades and vanes in modern aeroengines are mainly characterized by two-phase  $\gamma/\gamma'$  structures, in which  $\gamma'$  precipitates are coherently embedded in the  $\gamma$  matrix [1]. The temperature tolerance of current Ni-based SC superalloys is approaching 1100 °C. Any further drastic improvement of this temperature tolerance, however, would be difficult to achieve due to the relatively low melting point of Ni (1450 °C) in comparison with refractory elements. In the past few decades, the demand for high-efficiency, low-emission gas turbine technology has prompted the search for new materials with even higher temperature tolerances than the state-of-the-art Ni-based SC superalloys. Among the candidate materials, NiAl-based intermetallic compounds strengthened by coherent Ni<sub>2</sub>AlTi precipitates [2], W-based HfC dispersion-hardening alloys [3], and Nb-based Nb<sub>3</sub>Al precipitation-hardening alloys [4] exhibit high melting points, excellent oxidation resistance, and low density. However, applications of those alloys are limited due to their poor room temperature ductility. Recently, refractory Ir-based alloys have received increasing attention

because of their high melting temperature and good oxidation resistance [5–7]. Like Ni-based SC superalloys, Ir-based alloys have a two-phase  $\gamma/\gamma'$  structure, with  $\gamma'$  ( $L1_2$ ) precipitates coherently embedded in the FCC Ir  $\gamma$  matrix. According to binary phase diagrams of Ir–Ti and Ir–Ta [8, 9], the FCC Ir is in equilibrium with  $L1_2$   $Ir_3Ti$  and  $Ir_3Ta$  intermetallic compounds, respectively. Preliminary studies have shown that Ir-based alloys have attractive mechanical properties for ultrahigh-temperature applications [6, 7].

It is known that both single-phase solid solution  $\gamma$  and  $\gamma'$   $Ni_3Al$ -based intermetallic compounds are less resistant to creep deformation than two-phase  $\gamma/\gamma'$  superalloys [10]. The strength of two-phase  $\gamma/\gamma'$  alloys is not a simple linear sum of the strengths of the individual  $\gamma$  matrix and  $\gamma'$  precipitates. The interface between these two phases also plays an important role in controlling mechanical properties [11]. It is believed that the structure and properties of the  $\gamma/\gamma'$  interface greatly affect the shape, size, and coarsening rate of the  $\gamma'$  precipitates, which in turn are major factors influencing creep rupture strength of the alloys. Earlier experimental studies of Ir-based alloys were mainly focused on the microstructure and compressive strength. Recently, the flow behaviour and creep properties of the alloys have been investigated [12]. Considering the higher density ( $22.4 \text{ g cm}^{-3}$ ) and limit on resources, it is suggested that Ir-based alloys might be suitable for the aerofoil part of turbine vanes that is exposed to the highest temperatures, and for the higher-temperature side of functional-gradient composite materials in which Ni-based superalloys might be used for the lower-temperature side [7]. Despite these efforts, however, little is known about the  $\gamma/\gamma'$  interface structures and properties from the electronic structure point of view. Apparently, a complete understanding of the interface properties requires knowledge from electronic structure calculations. This paper presents our theoretical study of the electronic mechanism underlying the interface strength. Quantum mechanics calculations have been performed using the DMol3 (a type of density functional theory for molecules) molecular orbital approach. We start by calculating Mayer bond orders (MBOs) to evaluate the  $\gamma/\gamma'$  interface strength. Then we proceed to study the charge density distribution as well as charge transfer. The analysis includes the total valence charge density, bonding charge density, Hirshfeld charge [13], Mulliken orbital populations [14], and MBO [15]. An electronic mechanism responsible for the interface strength of Ir/ $Ir_3X$  ( $X = Ta, Ti$ ) alloys is then suggested from examining the bond order (BO), electronic structures, and charge density.

## 2. Computational method and model

We use a molecular cluster DMol3 approach to calculate the electronic structures of the model system. In general, a molecular cluster approach is suitable for studying electronic properties that are primarily a function of the local environment [16]. The double numerical basis set for Ir, Ti, and Ta atoms, which contains a double-set valence function, is employed, as this has proven to be very efficient in studying molecular cluster systems [16–18]. We use the frozen-core approximation for Ir, Ta, and Ti atoms in the calculations. The degree of convergence of the self-consistent iterations, measured by (rms) changes in the charge density, is set to  $10^{-5}$ , which allows the binding energy to converge to  $10^{-5}$  Ryd. All calculations in the present research are performed with the generalized-gradient approximation (GGA) proposed by Perdew and Wang [19].

Figure 1 shows a 63-atom cluster model for the  $\gamma/\gamma'$  interface of two-phase Ir/ $Ir_3X$  ( $X = Ta, Ti$ ) alloys. The cluster model consists of an upper Ir region and a lower  $Ir_3X$  region, representing the  $\gamma$  matrix and  $\gamma'$  precipitate in the two-phase alloys, respectively. In this paper, we define the 1–1 layer as the lowest plane of the upper Ir region, while the 0–0 layer is the highest plane of the  $Ir_3X$  region. The 0–0 layer ( $x$ – $y$  plane), as labelled in figure 1,

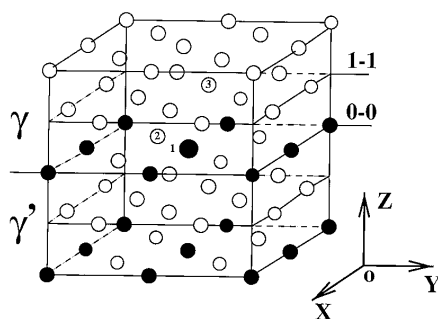


**Figure 1.** The cluster model for DMol calculations. Open circles: Ir atoms; black circles: Ti or Ta atoms. Numbers (1, 2, 3) in the cluster model represent inequivalent atoms based on the  $C_{4v}$  point group symmetry.

contains mixed Ir and X atoms, in which Ir atoms occupy the face-centre sites, while X atoms occupy the corner sites. Inequivalent atoms in the cluster, as shown in figure 1, are denoted by numerical labels based on the  $C_{4v}$  point group symmetry of the cluster. The lattice constants of the cluster are chosen to be equal for Ir ( $\gamma$ ) and  $\text{Ir}_3\text{X}$  ( $\gamma'$ ), in view of the assumption of complete interface coherence. The cluster is relaxed with the variation of the lattice constant when energetic calculations are performed.

### 3. Results and discussion

In order to investigate the electronic mechanism of the  $\gamma/\gamma'$  interface strength of Ir/ $\text{Ir}_3\text{X}$  alloys, we need to consider the values for the order of the bonds between atoms. The BO, in nature, is the overlap of electron wavefunctions between atoms, which can be used to quantitatively measure the strength of atomic bonding and thus assess the strength of an interface consisting of these atoms. Previous work [20–22] has shown that BOs could serve as predictors of interface strengthening and environmental embrittlement of intermetallic compounds on the basis of first-principles calculations. In this study, we use the MBO and calculational approach [15]. The definition of the MBO for bonds between atoms A and B is as follows:

$$\text{BO}_{\text{AB}} = 2 \sum_{\mu \in \text{A}} \sum_{\nu \in \text{B}} [(P^\alpha S)_{\mu\nu} (P^\alpha S)_{\nu\mu} + (P^\beta S)_{\mu\nu} (P^\beta S)_{\nu\mu}] \quad (1)$$

where  $P^\alpha$ ,  $P^\beta$  are the density matrices,  $S$  is the overlap matrix of the wavefunctions (see the details in [15]). We calculate  $\text{BO}_{\text{AB}}$  values for the first-nearest-neighbour (FNN) B atoms around the A site. Our calculations indicate that the  $\text{BO}_{\text{AB}}$  value is small if the separation between atoms A and B is beyond the FNN range, and thus can be neglected without altering the conclusions. In order to examine the interface strength, we divide the BOs into vertical and horizontal components. The vertical BO ( $\text{BO}^v$ ) is defined and calculated for atoms along the [001]  $z$ -direction to measure the cohesion strength of atoms across the  $\gamma/\gamma'$  interface. The horizontal BO ( $\text{BO}^h$ ), however, is defined and calculated for in-plane atoms perpendicular to the [001]  $z$ -direction. We define a local sum of BOs  $\sum \text{BO}^h$  within the 0–0 and 1–1 layers as the measure of the shear strength of the  $\gamma/\gamma'$  interface, while the local sum of BOs  $\sum \text{BO}^v$  across the 0–1 layer is the measure of the cohesion strength of the  $\gamma/\gamma'$  interface. It is demonstrated that this approach is not only easy to use for evaluating the interface strength, but also convenient for the examination of interface strengthening induced by other substitution elements [17, 18].

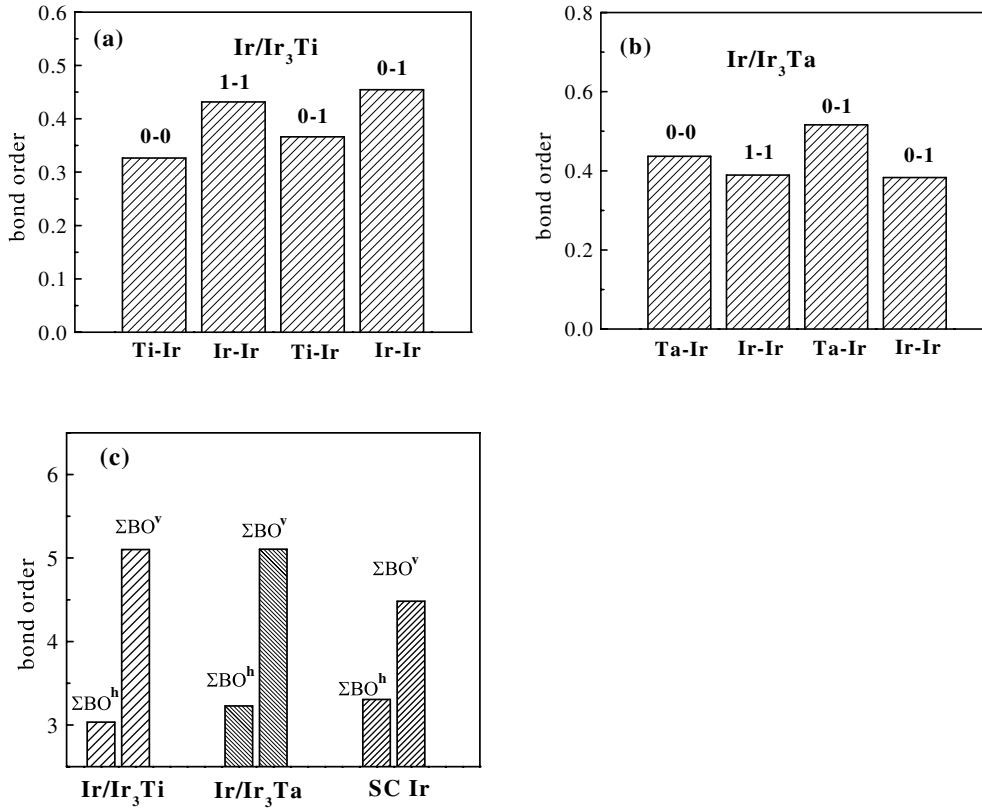


**Figure 2.** (a) BOs for the  $\gamma/\gamma'$  interface of Ir/Ir<sub>3</sub>Ti, and (b) BOs for the  $\gamma/\gamma'$  interface of Ir/Ir<sub>3</sub>Ta. 0–0 and 1–1 represent the BOs within the 0–0 ( $x$ – $y$ ), 1–1 ( $x$ – $y$ ), and 0–1 ( $x$ – $z$ ) planes, respectively. (c) BOs representing the shear, cohesion, and interface strengths:  $\Sigma BO^h$ ,  $\Sigma BO^v$  for Ir/Ir<sub>3</sub>X (X = Ti, Ta) and SC Ir.

The calculated BOs for Ir/Ir<sub>3</sub>X alloys are shown in figure 2. The order of the bonds between Ti and Ir atoms within the 0–0 layer, which is the top plane of the  $\gamma'$  Ir<sub>3</sub>Ti precipitate, is  $BO_{Ir-Ti}^h = 0.3266$ . Similarly, the order of the bonds between Ir atoms within the 1–1 layer, which is the bottom plane of the Ir  $\gamma$  matrix, is  $BO_{Ir-Ir}^h = 0.4371 > BO_{Ir-Ti}^h = 0.3266$ . This is possibly due to the Ir d/Ir d hybridization in the 1–1 plane being stronger than the Ir d/Ti d hybridization in the 0–0 plane. Using the above definition, the sum  $\Sigma BO^h = 3.0332$  within the two layers (0–0 and 1–1) can be used to measure the shear strength of the  $\gamma/\gamma'$  interface for Ir/Ir<sub>3</sub>Ti alloy, as shown in figure 2. Similarly, calculations show that  $BO_{Ir-Ti}^v$  across the 0–1 plane along the [001]  $z$ -direction is 0.3662, while  $BO_{Ir-Ir}^v$  in the same plane is 0.4546. This implies that the bonding between Ir atoms across the  $\gamma/\gamma'$  interface is stronger than that between Ti–Ir atoms. The cohesion strength of the  $\gamma/\gamma'$  interface given by  $\Sigma BO^v$  is 5.1016.

From similar calculations, figure 2(b) shows the BOs of the  $\gamma/\gamma'$  interface for Ir/Ir<sub>3</sub>Ta alloy. Firstly,  $BO^h$  for between Ir and Ta atoms within the 0–0 horizontal layer is 0.4368, which is larger than both  $BO^h$  for between Ir and Ti (0.3266) and  $BO^h$  for between Ir and Ir (0.4317) for Ir/Ir<sub>3</sub>Ti alloy. Secondly,  $BO^h$  for between Ir and Ir within the 1–1 layer of Ir/Ir<sub>3</sub>Ta is 0.3895, which is less than  $BO^h$  for between Ir and Ta atoms of the 0–0 plane. These results imply that the bonding between Ir and Ta atoms is stronger than that between Ir atoms for

both Ir/Ir<sub>3</sub>Ti and Ir/Ir<sub>3</sub>Ta, which can be attributed to the strong Ta d/Ir d electron hybridization. The shear strength of the  $\gamma/\gamma'$  interface of Ir/Ir<sub>3</sub>Ta measured by  $\sum BO^h$  is 3.3052, which is greater than that, 3.0332, for Ir/Ir<sub>3</sub>Ti.  $BO^v$  for between Ir and Ta atoms across the vertical 0–1 layer is 0.5106, larger than  $BO^v = 0.3828$  for between Ir atoms across the same layer. The strong Ir–Ta bonding is expected to cause strong interface cohesion for the Ir/Ir<sub>3</sub>Ta alloy. However, the cohesion strength of Ir/Ir<sub>3</sub>Ta determined by  $\sum BO^v$  is 5.1048, and therefore close to the value 5.1016 for Ir/Ir<sub>3</sub>Ti alloy. Further analysis reveals that although  $BO_{Ir-Ta}^v$  (0.5106) is larger,  $BO_{Ir-Ir}^v$  (0.3828) for Ir/Ir<sub>3</sub>Ta is less than  $BO_{Ir-Ir}^v$  (0.4546) for Ir/Ir<sub>3</sub>Ti alloy due to electron charge transfers. As a result, the combination of  $BO_{Ir-Ta}^v$  or  $BO_{Ir-Ti}^v$  with  $BO_{Ir-Ir}^v$  in the two alloys gives rise to similar interface cohesion strengths.

To further understand the influence of Ti and Ta on the interface properties, the ‘interface strength’ of SC Ir is calculated and compared with that of Ir/Ir<sub>3</sub>X (X = Ti, Ta). By substituting Ir atoms for Ti or Ta atoms in the  $\gamma'$  precipitates, a SC Ir model with an ‘Ir/Ir *conceptual interface*’ is constructed. BOs for Ir atoms located at the original Ti or Ta sites are calculated, to represent the ‘interface strength’. The calculated  $BO^h (=BO^v)$  for an Ir–Ir pair is 0.4035, and the symbol  $BO^{hv}$  is used to describe this value for convenience. The same definition of strength with BOs as the measure of the Ir crystal strength as in the preceding section is used. It is evident that  $BO^{hv}$  (0.4035) for SC Ir is larger than  $BO^h$  (0.3266) for Ir–Ti atoms within the 0–0 layer of Ir/Ir<sub>3</sub>Ti, but less than  $BO^h$  (0.4368) for Ir–Ta (0.4368) within the 0–0 layer of Ir/Ir<sub>3</sub>Ta. Similarly,  $BO^{hv}$  for SC Ir (0.4035) is larger than  $BO^v$  (0.3662) for an Ir–Ti pair in Ir/Ir<sub>3</sub>Ti, but less than  $BO^h$  (0.5106) for an Ir–Ta pair in Ir/Ir<sub>3</sub>Ta across the 0–1 plane. For Ir–Ir pairs in SC Ir and Ir/Ir<sub>3</sub>X alloys, it is found that  $BO^{hv}$  is less than  $BO^v$  (0.4546) and  $BO^h$  (0.4371) for Ir/Ir<sub>3</sub>Ti, and greater than  $BO^v$  (0.3832) for Ir/Ir<sub>3</sub>Ta. The shear and cohesion strengths of the ‘ $\gamma/\gamma'$  interface’ of SC Ir measured by  $\sum BO^v$  and  $\sum BO^h$  are 3.228 and 4.842, respectively. The cohesive and shear strengths of the  $\gamma/\gamma'$  interface measured by  $\sum BO^v$  and  $\sum BO^h$  for Ir/Ir<sub>3</sub>Ta are increased by 2.4 and 5.43% relative to SC Ir, respectively. The cohesion and shear strengths of Ir/Ir<sub>3</sub>Ti increase by 2.4% and decrease by 6.0%, respectively. Thus, it is useful to use the BO method to access the interface properties induced by element substitutions. Rice and Thompson [23] speculated that brittle versus ductile behaviour may be governed at the tip of an atomically sharp crack. A material will, in principle, fail in a brittle manner if the ideal cohesive strength is reached along the extension of the crack before the ideal shear strength is reached. Thus, according to Rice and Thompson theory, introducing a  $\gamma/\gamma'$  interface, in both Ir/Ir<sub>3</sub>X (X = Ti, Ta) alloys, promotes the ductile tendency as compared with pure SC Ir.

In order to further study the electronic mechanism underlying the  $\gamma/\gamma'$  interface strength of Ir/Ir<sub>3</sub>X alloys, the electronic charge distribution associated with the interfacial structure is investigated. Two types of charge density distribution are calculated, namely the total valence charge density  $\rho(r)$  and the bonding charge density  $\Delta\rho_B(r)$ . The latter involves the charge transfer and the formation of directional bonding due to Ir d/X d hybridization. The bonding charge density, which is referred to as the atomic charge density in the presence of a crystal field, is defined as the charge difference between  $\rho(r)$  for the cluster and  $\rho_\alpha(r)$  for the superposition of neutral Ir and X (Ta or Ti) atoms; i.e.,

$$\Delta\rho_B(r) = \rho_{\text{cluster}}(r) - \sum_{\alpha} \rho_{\alpha}(r - r_{\alpha}). \quad (2)$$

Figure 3(a) presents the total valence charge density contour plot of Ir/Ir<sub>3</sub>Ti on the 0–0 ( $x$ – $y$ ) horizontal plane in units of  $10^{-3} e \text{ au}^{-3}$ . Metallic bonding character is observed at the lattice sites. Figure 3(b) plots the total valence charge density distribution on the (010) ( $x$ – $z$ ) vertical plane. A metallic bonding character similar to that in figure 3(a) is also found. It is evident from the number of contour lines between atoms that the Ir–Ir bonding in the  $\gamma$  region above the  $\gamma/\gamma'$  interface is stronger than that between Ir–Ti atoms on the interface. This is consistent

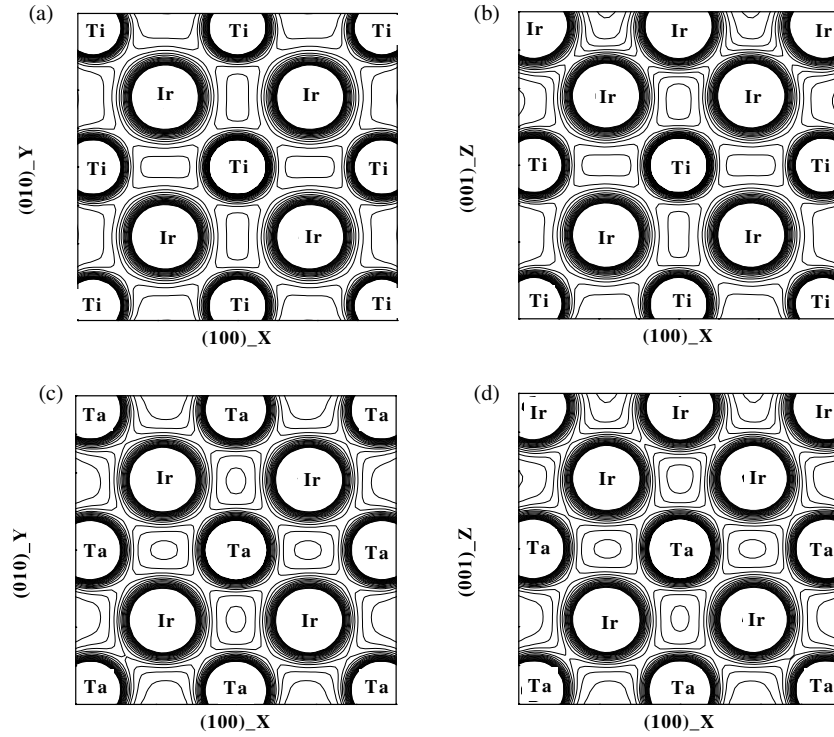


**Figure 3.** (a) The total valence charge density for the  $\gamma/\gamma'$  interface on the 0-0 ( $x$ - $y$ ) plane for Ir/Ir<sub>3</sub>Ti. Contours start from  $\pm 0.001 e \text{ au}^{-3}$ , and increase successively in steps of  $0.01 e \text{ au}^{-3}$ . (b) The total valence charge density for the  $\gamma/\gamma'$  interface on the 0-1 ( $x$ - $z$ ) plane for Ir/Ir<sub>3</sub>Ti. Contours start from  $\pm 0.001 e \text{ au}^{-3}$ , and increase successively in steps of  $0.01 e \text{ au}^{-3}$ . (c) The total valence charge density for the  $\gamma/\gamma'$  interface on the 0-0 ( $x$ - $y$ ) plane for Ir/Ir<sub>3</sub>Ta. Contours start from  $\pm 0.001 e \text{ au}^{-3}$ , and increase successively in steps of  $0.01 e \text{ au}^{-3}$ . (d) The total valence charge density for the  $\gamma/\gamma'$  interface on the 0-1 ( $x$ - $z$ ) plane for Ir/Ir<sub>3</sub>Ta. Contours start from  $\pm 0.001 e \text{ au}^{-3}$ , and increase successively in steps of  $0.01 e \text{ au}^{-3}$ .

with the BO calculations in the preceding sections. Figures 3(c) and (d) show the total valence charge density distributions of Ir/Ir<sub>3</sub>Ta on both 0-0 ( $x$ - $y$ ) horizontal and (010) ( $x$ - $z$ ) vertical planes. For comparison with figures 3(a) and (b), the same contour plot levels are employed. From the contour plots, we see that the bonding between Ir and Ta atoms on the 0-0 layer is stronger than that between Ir-Ti atoms of Ir/Ir<sub>3</sub>Ti on this same layer. However, as shown in figure 3(d), the Ir-Ir bonding and Ir-Ta bonding appear to be smaller than that between Ir and Ta atoms. More quantitative BO calculations show that  $\text{BO}_{\text{Ir-Ta}}^{\text{v}} = 0.5106$  and  $\text{BO}_{\text{Ir-Ir}}^{\text{v}} = 0.3828$  for Ir/Ir<sub>3</sub>Ta.

Figure 4(a) shows the bonding charge density distribution of the  $\gamma/\gamma'$  interface on the 0-0 layer of Ir/Ir<sub>3</sub>Ti. The solid and dashed curves denote the contour plots for increased (accumulation) and decreased (depletion) electronic charge density, respectively, as atoms are brought together to form the interface. We find a depletion of electron density at the Ti sites accompanied by a significant build-up of the directional d-bonding charge along the FNN Ir-Ti direction. The Ir-Ti bonding character is ionic in nature, with Ti atoms donating electrons, while Ir atoms gain electrons. Figure 4(b) illustrates the bonding charge density distribution of Ir/Ir<sub>3</sub>Ti on the (010) ( $x$ - $z$ ) plane across the  $\gamma/\gamma'$  interface. Like in figure 4(a), significant anisotropic directional bonding build-up around Ir sites occurs below the 0-0 layer in the  $\gamma'$



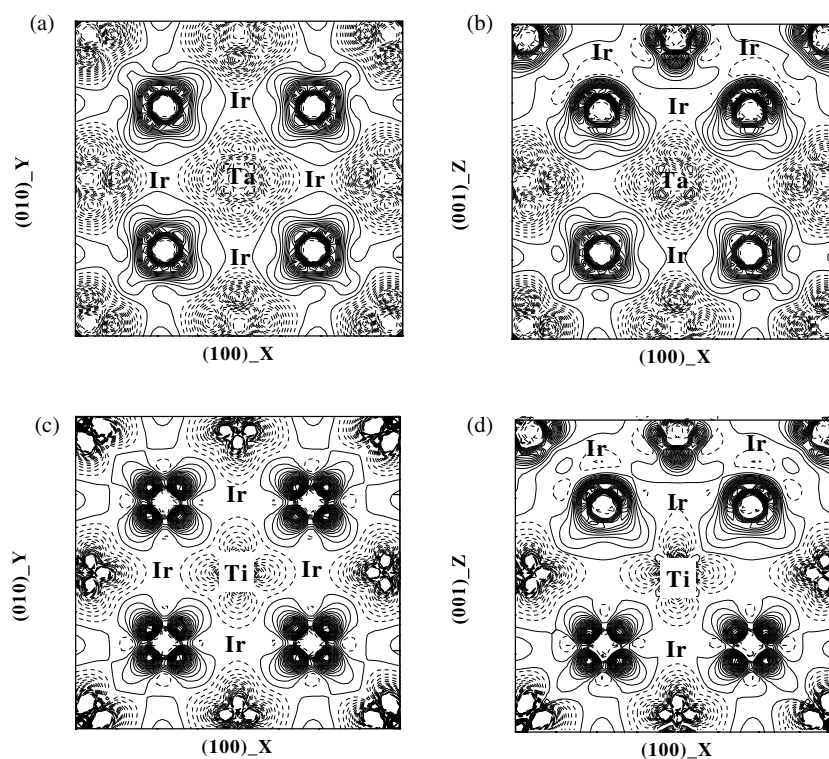


**Figure 4.** (a) The bonding charge density of the  $\gamma/\gamma'$  interface on the 0–0 ( $x$ – $y$ ) plane for Ir/Ir<sub>3</sub>Ti. Contours start from  $\pm 1.0 \times 10^{-3} e \text{ au}^{-3}$ , and increase in steps of  $5.0 \times 10^{-3} e \text{ au}^{-3}$ . (b) The bonding charge density of the  $\gamma/\gamma'$  interface on the 0–1 ( $x$ – $z$ ) plane for Ir/Ir<sub>3</sub>Ti. Contours start from  $\pm 1.0 \times 10^{-3} e \text{ au}^{-3}$ , and increase in steps of  $5.0 \times 10^{-3} e \text{ au}^{-3}$ . (c) The bonding charge density of the  $\gamma/\gamma'$  interface on the 0–0 ( $x$ – $y$ ) plane for Ir/Ir<sub>3</sub>Ta. Contours start from  $\pm 1.0 \times 10^{-3} e \text{ au}^{-3}$ , and increase in steps of  $5.0 \times 10^{-3} e \text{ au}^{-3}$ . (d) The bonding charge density of the  $\gamma/\gamma'$  interface on the (010) ( $x$ – $z$ ) plane for Ir/Ir<sub>3</sub>Ta. Contours start from  $\pm 1.0 \times 10^{-3} e \text{ au}^{-3}$ , and increase in steps of  $5.0 \times 10^{-3} e \text{ au}^{-3}$ .

precipitate. The bonding at Ir sites in the  $\gamma$  matrix on the 1–1 layer is towards FNN Ir–Ti atoms, and the unique symmetry axis for the charge distribution is the  $z$ -axis. Figures 4(c) and (d) show the bonding charge density distribution of Ir/Ir<sub>3</sub>Ti alloy on both 0–0 ( $x$ – $y$ ) horizontal and (010) ( $x$ – $z$ ) vertical planes. Like for Ir/Ir<sub>3</sub>Ti, a directional bonding character emerges in the bonding between Ir and Ta atoms with more significant anisotropic d-bonding character for the bonding around Ir atoms.

The Hirshfeld orbital population provides an effective way to quantitatively describe the charge accumulation or depletion around atoms as well as the charge transfers between orbitals [13]. Thus, it can be used to interpret the change associated with the interatomic bonding character. For the  $\gamma/\gamma'$  interface in Ir/Ir<sub>3</sub>X alloys, it is found that X atoms in  $\gamma'$  donate electrons, while Ir atoms gain electrons in terms of the charge density distribution, as shown in figure 4. Orbital calculations indicate that the 6s electrons of the Ta atom transfer to their 5d and 6p orbitals, while the 6s electrons of the Ir atom transfer to their 6p orbitals, leaving the electrons at 5d orbitals almost intact. This is one type of electronic structure of the  $\gamma/\gamma'$  interface for Ir/Ir<sub>3</sub>Ta. In the case of Ir/Ir<sub>3</sub>Ti, it is found that the 4s electrons of the Ti atom transfer to their 3d and 4p orbitals, while, as in the case of Ir/Ir<sub>3</sub>Ta, the 6s electron of



the Ir atom transfers to their 6p orbitals. Detailed orbital analysis demonstrates that although the 4s orbital electrons of the Ti atom transfer more electrons (1.354) to their 3d orbital than Ta (0.783) does, the total number of d electrons of the 3d orbital of the Ti atom is 2.783, which is less than the number (3.446) for the 5d orbital of the Ta atom. Consequently, the Ta d/Ir d d-bonding hybridization in Ir/Ir<sub>3</sub>Ta alloy is stronger than the Ti d/Ir d hybridization in Ir/Ir<sub>3</sub>Ti alloy. This is possibly why the interface shear strength of Ir/Ir<sub>3</sub>Ta is larger than that of Ir/Ir<sub>3</sub>Ti.

Ir-based alloys are promising materials for ultrahigh-temperature applications. A deeper understanding of the interface strength mechanism at the atomic level could be of tremendous importance to future alloy design. In this study, the BO<sup>h</sup> and BO<sup>v</sup> components have been calculated to evaluate the  $\gamma/\gamma'$  interface strength of Ir/Ir<sub>3</sub>X (X = Ti, Ta) alloys. Work currently in progress is investigating other Ir/Ir<sub>3</sub>X (X = V, Hf, Zr, Nb) alloys. We intend to proceed with calculations to assess the strengthening effects on the  $\gamma/\gamma'$  interface,  $\gamma$  matrix, and  $\gamma'$  precipitates.

#### 4. Conclusions

The electronic structures of the  $\gamma/\gamma'$  interface of Ir-based two-phase Ir/Ir<sub>3</sub>X (X = Ti and Ta) alloys have been investigated by means of first-principles DMol calculations. The underlying bonding mechanism responsible for the interface strength consists of the directional d bonding and the charge transfer from Ta or Ti atoms to Ir atoms. The sum of the MBOs is calculated, as a qualitative measure of the interface strength, and used to represent the interface strength. Results show that both the cohesive strength and the shear strength of Ir/Ir<sub>3</sub>Ta increase relative to those of SC Ir, while the shear strength of the interface for Ir/Ir<sub>3</sub>Ti decreases, and the cohesive strength increases. The introduction of the interface promotes the tendency to ductility of two-phase alloys.

#### Acknowledgments

The authors would like to acknowledge the financial support from the Department of National Defense (Canada) through the Technology Investment Fund Program, and by the National Research Council Canada Institute for Aerospace Research.

#### References

- [1] Sims C T 1987 *Superalloys* vol 2 (New York: Wiley)
- [2] Miracle D B and Darolia R 1995 *Intermetallic Compounds: Principles and Practice* vol 2, ed J H Westbrook and R L Fleischer (New York: Wiley) pp 53–72
- [3] Brown W F Jr, Mindin H and Ho C Y 1992 *Aerospace Structural Metals Handbook* vol 5 (West Lafayette, IN: INDAS/Purdue University) p 4218, 5502
- [4] Yamagata T 1994 *Proc. 5th Symp. on High-Performance Materials for Severe Environments (Tokyo)* (Tokyo: RIMCOF) pp 107–14
- [5] Yamabe Y, Koizumi Y, Murakami H, Ro Y, Maruko T and Harada H 1996 *Scr. Metall. Mater.* **35** 211
- [6] Yamabe Y, Koizumi Y, Murakami H, Ro Y, Maruko T and Harada H 1997 *Scr. Metall. Mater.* **36** 393
- [7] Yamabe-Mitarai Y and Harada H 2002 *Phil. Mag. Lett.* **82** 109
- [8] Hansen M 1958 *Constitution of Binary Alloys* (New York: McGraw-Hill)
- [9] Shunk F A 1969 *Constitution of Alloys* Suppl.2 (New York: McGraw-Hill)
- [10] Ro Y, Koizumi Y and Harada H 1997 *Mater. Sci. Eng. A* **223** 59
- [11] Yamabe Y, Ro Y, Maruko T and Harada H 1998 *Metall. Trans. A* **29** 537
- [12] Gu Y F, Yamabe-Mitarai Y, Nakazawa S and Harada H 2002 *Scr. Mater.* **46** 137
- [13] Hirshfeld F L 1977 *Theor. Chim. Acta* **44** 129
- [14] Mulliken R S 1955 *J. Chem. Phys.* **23** 1833

- 
- [15] Mayer I 1986 *Int. J. Quantum Chem.* **29** 477
  - [16] Tang S P, Freeman A J and Olson G B 1993 *Phys. Rev. B* **47** 2441
  - [17] Chen K, Zhao L R and Tse J S 2002 *Phil. Mag. A* at press
  - [18] Chen K, Zhao L R and Tse J S 2002 *Phil. Mag. Lett.* at press
  - [19] Perdew J P and Wang Y 1986 *Phys. Rev. B* **33** 8800
  - [20] Lu G, Gu J T, Chen K and Hu Z Q 1996 *Acta Mater.* **44** 4019
  - [21] Liu Y, Chen K, Zhang J and Hu Z Q 1997 *J. Phys.: Condens. Matter* **9** 9829
  - [22] Liu Y, Chen K, Zhang J H and Hu Z Q 1998 *J. Mater. Res.* **13** 290
  - [23] Rice J and Thomson R 1974 *Phil. Mag.* **29** 73